Simplified Analytical Approximations for Scaled Composite Laminates under Transverse Loading

XC Sun*[a], S R Hallett[a], H Suemasu[b], M R Wisnom[a]

[a] University of Bristol, Queen's Building, University Walk, Bristol BS8 1TR, UK
[b] Department of Mechanical Engineering, Sophia University, 7-1 Kioi-cho, Chiyoda-ku, Tokyo 105-8554, Japan

Abstract

Delaminations caused by impact or indentation are a major cause of strength reduction in composite laminated structures. Since delaminations seldom occur in just one location through the thickness, the effect of multiple delaminations on the geometrical nonlinearity and response of scaled composite laminated plates subjected to a transverse concentrated load is studied here through analytical formulations. The scaling includes in-plane dimension scaling and sublaminate scaling based on a Reference plate with a stacking sequence of $[45^o/90^o/0^o/\text{-}45^o]_{2S}$. The analytical approximation obtained under point loading quasi-static indentation is also suitable for studying large-mass low-velocity impact or for experiment and laminate design. The analytical approximations were compared with axisymmetric finite element model and static indentation tests conducted in a previous study. The novel achievement of this work is that it includes analytical expressions to predict the evolution of damage and load-displacement curves as a simpler alternative to the complex nonlinear finite element models.

Keywords: Impact Damage, Energy release rate, Analytical approximation, Finite element analysis.

1 Introduction

The use of composite structures has increased in many industries because of their advantage in weight reduction and advanced mechanical properties over traditional metal alloys. However, due to lack of reinforcement in the though thickness direction of laminated composites, they become vulnerable under out-of-plane (or transverse) loading, where interlaminar shear stresses develop. Amongst all transverse loading scenarios, static indentation and low-velocity impacts, that can induce Barely Visible Impact Damage (BVID), receive the greatest design consideration. This is because internal delamination damage, that is

* Author to whom correspondence should be addressed. Email: ric.sun@bristol.ac.uk

not easily visible from the structures' surface, can grow under continuous loading, leading to catastrophic structure failure especially under compressive loading [1]. As this is an important factor in design considerations, many studies use analytical or numerical approaches to predict the structural response and damage of composites under transverse loading to understand the system kinematics and material failure mechanisms.

Numerical approaches provide full-field accurate solutions for such loading scenarios. With the help of commercial finite element packages and various material failure models, the nonlinear structural response, material damage behaviour and failure mechanisms can be modelled, validated and predicted. Studies such as found in references [2–7] used continuum or discrete approaches to predict inter- and intraply damage of laminated composites under static indention or low-velocity impact, and their modelling results were validated against experimental observations with good correlations. Numerical modelling is in general accurate and suitable for structural level analysis and for investigating detailed damage behaviour. However, time spent for pre- and post-processing and CPU run times makes these methods relatively slow compared to analytical approaches.

In contrast, analytical modelling uses closed form expressions from classic theories i.e. Classic Laminate Theory (CLT), thin plate or shell theory, contact theories, solid mechanics, instead of applying computational mechanics. The advantage of analytical modelling over numerical modelling is that it provides insights on the governing parameters of impact response and identifies damage initiation, providing better understanding of the damage mechanisms during impact with considerably less computational effort. However, analytical approximations are not able to be simulate geometric nonlinearity for complex structures in most of the cases. In addition, one of the major limitations of most analytical models is that they are only available for laminate response in the elastic regime and up to damage initiation but do not take damage growth into account due to the complexity of the stress state in composite laminates. However, such difficulties can be avoid by using sensible homogenisation methods and non-dimensionalisation [8]. In low-velocity impact modelling, the analysis is generally assumed to be a quasi-static process and equivalent to static indentation [9]. Analytical study of impact on composites can be broadly categorised into four methods, as follows:

1. Analysing impact response through local deflection, using various contact laws in conjunction with experimental static indentation laws

1. Using discrete spring-mass model to predict elastic response of a laminate during impact
2. Analytically derived damage thresholds (or failure criteria) for the BVID

Since the laminate response during impact is a complex process and varies with the physical configuration of the laminate, impactor, boundary conditions, and impact energies, it is important to understand and generalise the behaviour of laminates into different types of impact. The information can then be used for predicting the resulting damage incurred. Olsson [10] defined three impact types based on impactor velocity, and the mass of the impactor and substrate. Similar studies in the literature include those of Christoforou and Yigit [11], Abrate [9] and Lin and Fatt [12]. Some early studies [13–15] used the modified Hertzian contact law in the loading phases and a power law in the unloading phase to characterise the relationship between contact load and indentation in different laminates under transverse loading. They suggested that the contact force is proportional to the transverse modulus and that the contact law is significantly influenced by the indentation level and the deflection of the laminate; as indentation and the curvature of the laminate increase, the effects of the large contact area and membrane stiffening on contact stress redistribution lead to deviation from the Hertzian contact law in the experimental results [15]. Suemasu et al [16] used a superposition approach between local indentation derived by the contact law and forced vibration as a Boussinesq problem to study the force-indentation relationship of a transversely isotropic plate; the analytical results were in agreement with numerical FE solutions. In more recent studies [17,18], both qualitative and quantitatively predictions on the maximum force incurred during impact and the region at which it acts and the corresponding stress states everywhere inside the laminate, even with damage, were derived analytically. These were analysed by using a modified Hertzian contact pressure distribution together with plate theory, using numerical formulations to capture relatively detailed impact response and damage mechanisms in a circular plate under transverse loading. Due to the complexity of the calculations, most of the analytical studies available in the literature do not account for the evolution of contact stiffness with laminate deflection and the development of impact damage.

The most applicable analytical solution for delamination failure to the current work, the critical load for delamination initiation, was developed by Suemasu and Majima [8] and Davies et al. [19] based on linear elastic fracture energy. The case of multiple delaminations induced during low velocity impact of composite plate has been simplified to a problem of a single delamination and two ‘bonded’ axisymmetric beam-like plates under transverse point loading.

This prediction has been comprehensively verified and has been made use of in numerous experimental, analytical and FE modelling studies [20–23].

In this work, the complete force response of scaled laminates under static central transverse loading up to elastic, damage initiation and then in the growth regime was modelled. The governing parameters of damage growth and geometric nonlinearity due to damage growth were investigated using a nonlinear analytical solution. This method is based on fracture energy and thin homogenised plate mechanics under point loading with the assumptions that are otherwise similar to those in the linear analysis of Davies et al. [19] that considered only a single delamination. The occurrence of multiple delaminations is considered in this work, which is necessary to capture the full evolution of damage and the load curves, beyond the point of initiation. The laminate is modelled as a thin circular plate with fully-fixed boundary conditions at its edge. This arrangement allows one to perform axisymmetric finite element analysis to validate the proposed nonlinear analytical approximations. The preliminary analytical method was introduced previously [24], and is further developed and validated in this study. The experimental observations obtained in [6] are compared in detail with the predictions of the new analysis. This study demonstrates the predictive capabilities of the analytical modelling on the response of the composite under transverse loading and the scaling effects of laminates under transverse load. A superposition method is also developed here to model for the first time the complete load-displacement curves of scaled laminates under transverse loading with damage progression, as well as the load drop in the force-displacement relation indicating unstable delamination propagation.

2 Description of Analytical Model

A brief background of this approach is introduced here for the sake of completeness but is not elaborated in detail. The preliminary formulation can be found in [24]. For the case of a laminate under transverse loading, the deflection profile and underlying delaminated region are easily identifiable. The plate can then be divided into two portions. One is the intact (or 'undamaged') plate without delamination. The other is the damaged portion with multiple delaminations, as shown in Figure 1. It is assumed that the multiple delaminations cover a full circular area, with radius 'a', and are uniformly distributed through the thickness of the laminate, situated between two neighbouring sublaminates [$45^o_n/90^o_n/0^o_n/\text{-}45^o_n$] (See cross-section A'B'C'D' in Figure 1). The delaminated part therefore can be modelled as a circular plate with N sublaminates and N-1 circular delaminations.

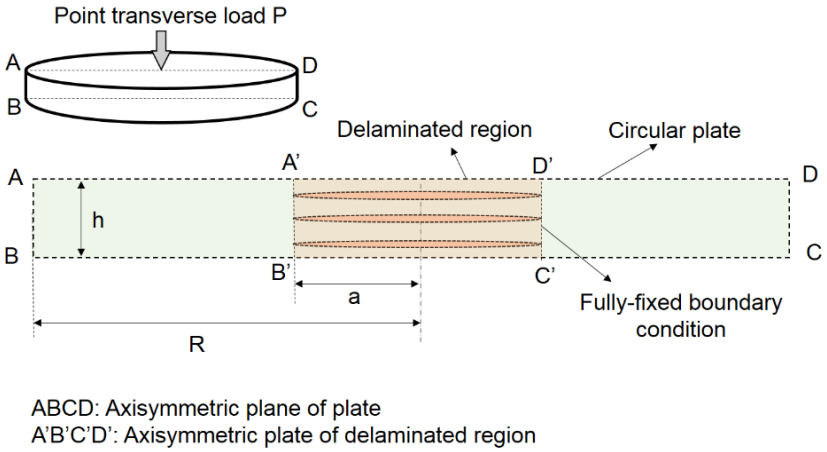

Figure 1: Illustration of circular plate under transverse point loading with multiple delamination formed at the centre of the plate.

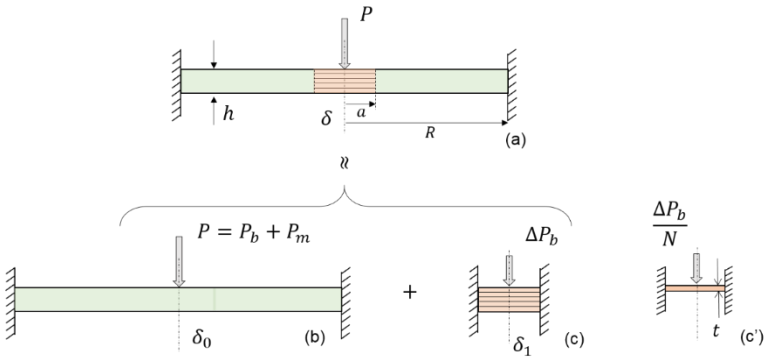

Figure 2: A circular plate with multiple circular delaminations subjected to a concentrated load at its centre can be expressed as superposition of three problems [23]. (a) circular plate with radius R containing N-1 number of delaminations with radius of a, (b) intact plate, (c) delaminated portion, (c') individual sublaminate.

The superposition technique is applied to describe the overall central mid-plane deflection of the plate. This superposition consists of two components: an intact ('undamaged') plate with nonlinear response subjected to a concentrated load at its centre, a circular plate with radius '*a*' and a thickness the same as that of the delaminated portion. The delaminated portion is fixed at its periphery connecting to the intact plate, and they both are subjected to the same central point load. Cross-section views, corresponding to cross-section ABCD and A'B'C'D' in Figure 1, of the damaged plate and the displacement superposition mechanics are shown in Figure 2.

2.1 Displacement and Load Superposition

If considering a circular quasi-isotropic laminate with radius *R* and overall thickness *h* subject to a fully-fixed boundary condition, when the plate with the *N*-1 multiple circular delaminations of radius *a* is loaded at its centre as shown in Figure 2a, the damaged portion

significantly deforms and exhibits large geometric nonlinearity, whereas the deflection of the intact portion is relatively small and under the elastic regime, with only a slight geometric nonlinearity. The simple expression for the deflection of a plate under transverse loading is governed by two parameters; bending-shearing stiffness and membrane stiffness [25]. The flexural stiffness of a plate is proportional to the cube of the thickness (h^3). Assuming the uniformly distributed N-1 multiple delaminations divide the whole damaged portion into N sublaminates with equal individual thickness (t), then the flexural stiffness is reduced to the sum of the flexural stiffness of the N sublaminates. This is expressed as $1/N^2$ of the flexural stiffness of the intact plate. Due to fact that the membrane stiffness is proportional to the first order of the thickness (h), the reduction caused by multiple delaminations in the total membrane stiffness of the intact plate is assumed to be negligible. The overall response of a delaminated plate under transverse loading can be simplified by the superposition of three scenarios (b), (c) and (c') in Figure 2. The sum of the applied load (P) of the three scenarios is the same as that of scenario (a) in Figure 2.

In scenario (b), it is assumed that the shear stress distribution through the thickness at the delaminated surfaces is equal to that in the intact plate at the corresponding interfaces. The solution of scenario (b) is therefore simplified to the same as an intact plate. Then, the applied load can be decomposed into the linear bending load (P_b) and the nonlinear membrane load (P_m) components. Note that the nonlinearity in the plate response is with respect to the central deflection. Scenario (c) has N circular panels (delaminated sublaminates) with a radius of 'a' and a fully fixed boundary condition at delamination periphery. All the delaminated sublaminates are assumed to deflect together and have the same deflection. Because the change of membrane stiffness is negligible, the load required for the delaminated sublaminates to generate the same deflection as the intact plate reduces at the same rate as the bending stiffness. For a given deflection level, the load corresponding to the bending stiffness reduction (ΔP_b) can be written as:

$$\Delta P_b = P_b \left(1 - \frac{N D_d}{D_0}\right) \tag{1}$$

where D_0 and D_d are the bending rigidities of intact laminate and individual sublaminates (subscript '0' and 'd' to denote the intact and damaged states). ΔP_b results in local deflection δ_1 at the delaminated portion, as shown in Figure 2c. If the plate is assumed to be homogenised to an equivalent isotropic plate, $D_d = D_0/N^3$.

If there is no constraint between the delaminated surfaces and *the* sublaminates have the same deflection, then the overall deflection of a delaminated laminate (see Figure 2a) becomes equal to the sum of the two individual nonlinear component plates, namely the global intact plate (see Figure 2b) with radius 'R' and the local delaminated sublaminates with radius 'a' (see Figure 2c').

2.2 Non-dimensionalisation

The load-displacement relation of the global intact plate in scenario (b) is independent of the presence of multiple delaminations. A non-dimensional relation of the intact plate based on thin plate theory can be expressed as:

$$p_0 = q_0 + kq_0{}^{\gamma} \tag{2}$$

where k is a dimensionless coefficient of the nonlinear term relating to the geometry and mobility of the plate and it can be assumed that it is consistent in the global intact plate and in the local damaged portion. Factor γ is also a dimensionless factor that controls the level of nonlinearity of the plate, as previously stated, it is normally close to '3'. Both non-dimensional coefficients k and γ can be numerically determined by layered shell finite element analysis. The normalised load p_0 and displacement q_0 are defined as follows:

$$\begin{aligned} p_0 &= \frac{\psi P R^2}{16\pi D h} \\ q_0 &= \frac{\delta_0}{h} \end{aligned} \tag{3}$$

And the normalising term $R^2/16\pi Dh$ comes from thin plate theory, assuming linear deflection of a solid circular plate with fully constrained edges under a concentrated load [26].

Using the assumptions made earlier, the boundary of the local additional multiple delamination deformation shown in Figure 2c' can be fixed at the delamination periphery to the global plate. Then, the same relation is applied to the single circular plate with radius of 'a', and the relation between a non-dimensional local load p and a normalised local displacement q can be derived:

$$p = q + kq^{\gamma} \tag{4}$$

where

$$p = \frac{\Delta P_b a^2}{16\pi D_d t} \tag{5}$$

$$q = \frac{\delta_1}{t}$$

where t denotes the thickness of individual sublaminate and equal to h/N.

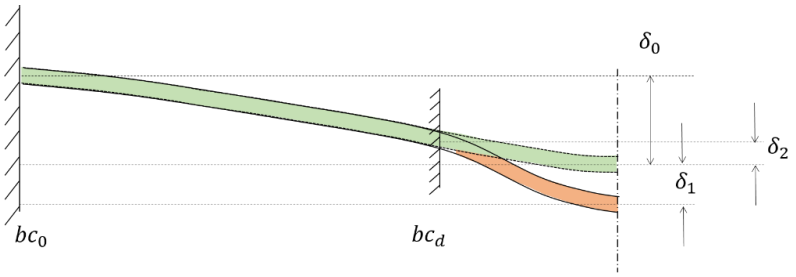

Figure 3: Local ply-level deflection components of damaged portion and global plate.

Because the starting point for the local deflection at the damaged portion (δ_1) is in the globally deformed frame, as shown in Figure 3, the initial global deflection level (δ_2) in the damaged frame (bc_d in Figure 3) needs to be taken into account in the overall load-displacement relation. This additional displacement in the bc_d frame, from the global deformation in the bc_0 frame, is the difference in displacement of the intact plate centre and the delamination boundary (see Figure 3) and can be expressed by normalisation $s = \delta_2/t$. The additional normalised load p can be considered as the load resulting in δ_1 that is the difference between the normalised load resulting in deflection $\delta_1 + \delta_2$ and that resulting in δ_2, which gives:

$$p = \{(q+s) + k(q+s)^\gamma\} - (s + ks^\gamma) = q + k\{(q+s)^\gamma - s^\gamma\} \tag{6}$$

$$s = \frac{\delta_2}{t} \tag{7}$$

Eq.6 and Eq.7 sufficiently explain the nonlinear relationship between the load and displacement of the damaged plates [23]. From linear solutions of an isotropic plate [22,26], s can be written as follows:

$$s = Nq_0\alpha^2(1 - 2\,ln\,\alpha) \tag{8}$$

where α is the non-dimensional delamination radius, $\alpha = a/R$. The bending load reduction ΔP_b due to multiple delaminations can be given as a linear expression with global non-dimensional deflection q_0 as follows:

$$\Delta P_b = \frac{16\pi D_0 h}{\psi R^2}\left(1 - \frac{1}{N^2}\right) q_0 \tag{9}$$

And the normalised local load p due to the bending stiffness reduction is derived as a linear function of q_0 using the same normalising method as for the intact plate:

$$p = \frac{N^3 a^2}{16\pi D_d} \Delta P_b = \frac{1}{\psi} N(N^2 - 1)\alpha^2 q_0 \tag{10}$$

Then, substituting Eq.10 into Eq.6, gives

$$q + k\{(q+s)^\gamma - s^\gamma\} = N(N^2 - 1)\alpha^2 q_0 \tag{11}$$

Up to here, three normalised deflection functions for the undamaged plate q_0 are available; the delaminated deflection starting from global deformation q, the transverse distance s representing the relative normalised displacement between the global deformed plate centre and the delamination boundary (i.e. at delamination size 'a'). Therefore, the term q_0 is a function of q and s, s is a function of q_0, and q is a function of both s and q_0. Figure 3 can thus be fully described by those non-dimensional terms.

2.3 Deriving Strain Energy Release Rate

When the size of the damage is constant, the complementary energy (Π_C) can be calculated by integrating the displacement δ (i.e. $\delta_0 + \delta_1$) with respect to the overall applied load P. The expression is:

$$\Pi_C = \int_0^P \delta \, dP = \int_0^P \delta_0 dP + \int_0^P \delta_1 \, dP = \Pi_{C0} + \Pi_{C1} \tag{12}$$

where Π_{C0} and Π_{C1} are complimentary energy of undamaged laminate and that of sublaminates, respectively, corresponding to the localised deformation. Considering the relationships between the global load and displacement in Eq.2, each term of the strain energy can be written as follows:

$$\begin{aligned} U_0 &= \frac{16\pi D h^2}{\psi R^2} \int_0^{q_0} q_0 \frac{dp_0}{dq_0} dq_0 = \frac{16\pi D h^2}{\psi R^2} \left(\frac{1}{2} {q_0}^{\gamma-1} + k^{¾} \, {q_0}^{\gamma+1} \right) \\ U_1 &= \frac{16\pi D h^2}{\psi N R^2} \int_0^{q_0} q \frac{dp_0}{dq_0} dq_0 = \frac{16\pi D h^2}{\psi N R^2} \int_0^{q_0} q(1 + 3k{q_0}^{\gamma-1}) dq_0 \end{aligned} \tag{13}$$

where q_0 can be considered as the final deflection of the global intact plate.

As U_0 is independent of the damage, the strain energy release rate of uniform growth of all delaminations can be given by differentiating the strain energy U_0 with respect to the sum of the N-1 incremental delamination areas '∂A'.

$$G = \left[\frac{\partial U_1}{\partial A} \right]_{P=const} = \left[\frac{\partial U_1}{2\pi a(N-1)\partial a} \right]_{P=const} = \left[\frac{\partial U_1}{2\pi \alpha R^2 (N-1)\partial \alpha} \right]_{P=const} \tag{14}$$

$$= \frac{1}{N(N-1)} \frac{8Dh^2}{\psi R^4} \int_0^{q_0} \frac{1}{\alpha} \left[\frac{\partial q}{\partial \alpha}\right]_{P=const} (1 + \gamma k {q_0}^{\gamma-1}) dq_0$$

$$q + k\{(q+s)^\gamma - s^\gamma\} = \frac{1}{\psi} N(N^2-1)\alpha^2 q_0 = g(q, s, \alpha) \tag{15}$$

Differentiating both sides of Eq.15 by α under the condition of constant P, the following relation is derived after some manipulation.

$$\frac{\partial q}{\partial \alpha} \frac{1}{\alpha}_{P=const.} = q_0 \frac{2\frac{1}{\psi} N(N^2-1) - \left(\frac{\partial g}{\partial s}\right)\left(\frac{1}{\alpha}\frac{\partial g}{\partial \alpha}\right)}{\frac{\partial g}{\partial q}} \tag{16}$$

where

$$\frac{\partial g}{\partial q} = 1 + \gamma k (q+s)^{\gamma-1}$$
$$\frac{\partial g}{\partial s} = \gamma k \{(q+s)^{\gamma-1} - s^{\gamma-1}\}$$
$$\frac{\partial g}{\partial \alpha} = -4N q_0 \alpha \, ln\, \alpha$$

Substituting Eq.15 into Eq.14 yields a normalized strain energy release rate Γ with normalising term $(8Dh^2)/R^4$ as follows:

$$\tilde{G} = \frac{G_{II}}{\left(\frac{8Dh^2}{R^4}\right)} = \frac{2(N+1)}{\psi} \int_0^{q_0} \frac{1 - \frac{2\, ln\, \alpha}{N^2-1} \psi \gamma k \{(q+s)^{\gamma-1} - s^{\gamma-1}\}}{1 + \gamma k (q+s)^{\gamma-1}} q_0 (1 + 3k {q_0}^2) dq_0 \tag{17}$$

The normalized strain energy release rate $\tilde{G}$ value can be derived by integrating Eq.17 numerically. Since q and s are functions of q_0, and q_0 is related to the applied load p_0, $\tilde{G}$ is a function of q_0 and, in turn, the transverse load. When $\tilde{G}$ is equal to unity, that is when the condition $G_{II} = G_{IIC}$ is met in Eq.17, the equilibrium path of load, P (from Eq.2 & 3), and overall displacement, δ (i.e. $\delta_0 + \delta_1$) derived from q and q_0, can be obtained numerically with increasing delamination size a. When the strain energy release rate is equal to the fracture energy, the expressions of the load and the displacement are as follows:

$$P_{cr} = \frac{16\pi Dh}{R^2} p_{0cr} = \frac{16\pi Dh}{R^2} (q_{0cr} + k {q_{0cr}}^\gamma)$$
$$\delta = h\left(q_{0cr} + \frac{q_{cr}}{N}\right) \tag{18}$$

3 Implementation to Scaled Plates

Table 1: Characteristics of four types of specimens used in this study

Case	Lay-up	In-plane dimensions (mm)	Thickness (mm)
Reference (Ref)	$[45^o/0^o/90^o/-45^o]_{2S}$	75 x 50	2
In-plane Scaling (Is)	$[45^o/0^o/90^o/-45^o]_{2S}$	150 x 100	2
Ply-blocked Scaling (Ps)	$[45^o_2/0^o_2/90^o_2/-45^o_2]_{2S}$	150 x 100	4
Sublaminate scaling (Ss)	$[45^o/0^o/90^o/-45^o]_{4S}$	150 x 100	4

Variations of the full expression (Eq. 17) can be applied to scaled plates that were investigated experimentally in a previous study [6]. The scaled plates were made using carbon /epoxy system IM7/8552 manufactured by Hexcel™, with layups and dimensions given in Table 1. It can be seen that these laminates present different scaling methods which can be compared in different scaling pairs. The Reference (Ref) and in-plane dimension scaled (Is) are one scaling pair (in-plain dimensions only); the Ref and Ply blocked scaled (Ps) plates are the fully scaled pair (all dimensions including ply block thickness); the Ref and Sublaminate scaled (Ss) plates are the direct scaling pair without ply thickness scaling; and the Ps and Ss is the ply thickness scaling only.

3.1 Linear solution

Depending on the required output, a full analysis based on Eq.17 may not provide the greatest benefits from the analytical study as it can be even less efficient than simplified FE analysis. In order to identify the key driving parameters small and non-critical terms and factors can be removed from the full expression, but these depend on the properties of the laminate. For thicker laminates in this work, such as the Ps and Ss cases under low-velocity impact or static indentation loading, the bending stiffness is considerably larger than the membrane stiffness. Laminates usually reach the critical state before geometric nonlinearity effects in the intact plate become significant. If considering only up to damage initiation, the nonlinear terms of the intact plate can be neglected. When the nonlinear terms associated with membrane stiffness of the global plate and delaminated portion are removed, Eq. 2 and 4 become $p_0 = q_0$ and $p = q$, respectively. Also neglecting the nonlinear membrane terms associated with higher order components, Eq.17 simplifies to the following:

$$\tilde{G}_{linear} = 2(N+1)\int_0^{q_0} q_0 dq_0 = (N+1){q_0}^2 \Rightarrow G_{linear} = \frac{P^2}{32\pi^2 D}(N+1) \qquad (19)$$

The right hand side equation of Eq. 19 coincides with the theoretical solution given in [8] for a linear circular plate under transverse loading. The geometric nonlinearities associated with a global intact plate and delaminated portion are important after the delamination initiation. The above expression may also be useful to determine the influencing factors at the critical state. Considering N = 2, that is, delamination occurring only at the mid-plane of the plate, Eq.19 reduces to the analytical expression in [19] that is ${P_{cr}}^2 = 8\pi^2\, Eh^3\, G_{IIC}/9(1-\upsilon^2)$ where P_{cr} is the critical load for delamination.

3.2 Thick laminate with multiple delaminations

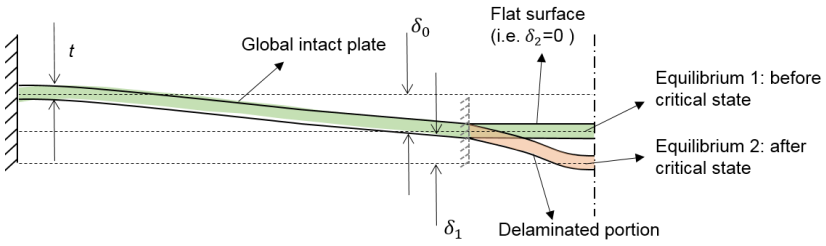

Figure 4 Deflection mechanics of a circular ply with delaminated portion. The central deflection at the delaminated region in intact plate is assumed as a flat surface.

Due to the linearity of the solution for thick laminates up to damage initiation, as described above, terms with higher order of q_0 can be assumed to be equal to zero. In addition, '*s*' as the distance between central deflection of the global intact plate and the deflection level at the location where the local deformation starts, can also be ignored. The term '*s*' associated with the damaged region initial deformation, thus coincides with the deformed shape of the undamaged plate. It becomes significant if the nonlinear term of the undamaged plate and the damage propagation are considered. This can be explained by the observation that CT-images and high-fidelity finite element models show the region immediately beneath the impactor/indenter to be free of delamination [6], due to the interlaminar shear stresses decreasing to zero at the centre of the laminate. There is also a strong indentation effect in laminates under transverse loading, and the region beneath the impactor is nearly a flat surface (See Figure 4). If $s \approx 0$, then the corresponding Eq. 8 does not hold anymore and Eq.6 and Eq.4 become equivalent. $s \approx 0$ also means that the terms $(\partial g/\partial s)(\partial g/\partial \alpha)(1/\alpha)$ can be neglected in Eq.16. After some manipulation the expression below can be obtained for the strain energy release rate G, which under the growth condition equals G_{cr}.

$$G = \frac{8Dh^2}{a^4(N-1)N^2(N^2-1)}\left(q^2 + \frac{1}{2}kq^4\right) = G_{cr} \tag{20}$$

Solving for the non-dimensional local deflection, q, at the growth condition can be written as follows:

$$kq^4 + 2q^2 - \frac{(N-1)N^2(N^2-1)a^4}{4Dh^2}G_{cr} = 0$$

$$q = \sqrt{\sqrt{\frac{1}{k^2} + \frac{N^2(N-1)^2(N+1)a^4G_{cr}}{4kDh^2}} - \frac{1}{k}}$$

$$= \sqrt{\frac{N^2(N-1)^2(N+1)\alpha^4(G_{cr}R^4/4Dh^2)}{\left\{\sqrt{1 + N^2(N-1)^2(N+1)k\alpha^4(G_{cr}R^4/4Dh^2)} + 1\right\}}} \tag{21}$$

Substituting $p = q + kq^\gamma$ into Eq.11 then gives

$$P_0 = \frac{16\pi Dh}{N(N^2-1)a^2}p = \frac{16\pi Dh}{N(N^2-1)a^2}(q + kq^\gamma) \tag{22}$$

Total displacement $\delta = \delta_0 + \delta_1$ can be calculated from:

$$\delta_0 = \frac{R^2P_0}{16\pi D} \tag{23}$$

$$\delta_1 = \frac{h}{N}q = \sqrt{\frac{(N-1)^2(N-1)a^4G_{cr}}{4D\left\{\sqrt{1 + \frac{N^2(N-1)^2(n+1)ka^4G_{cr}}{4Dh^2}} + 1\right\}}} \tag{24}$$

4 Finite Element Model Descriptions

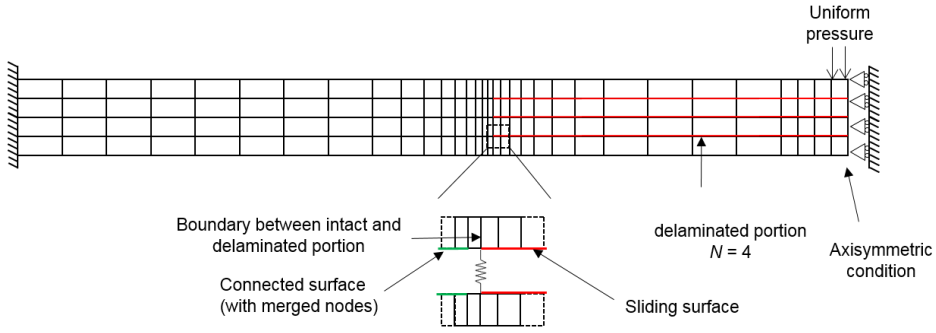

Figure 5: Schematic of axisymmetric finite element model.

Simple finite element simulations using axisymmetric elements were performed to evaluate and improve the approximations given by the present closed form solutions. The finite element models are based on the same assumptions made for the analytical solution and the

circular plate structure shown in Figure 5. Model descriptions are briefly presented in the following.

The model uses axisymmetric elements with area weighted mass definition (ELFORM 14 in LS-Dyna), and the material is modelled with isotropic material properties, which is consistent with the assumption of the analytical solutions. Figure 5 shows a schematic of the axisymmetric finite element model. To avoid problems due to a singularity in the model, the transverse point load assumption in the analytical solution is modelled by a uniformly distributed pressure load over 5% of the full span of the plate at the tip of the axisymmetric model, as shown in Figure 5. Cases when $N = 4$ and $N = 8$ are considered, and each case contains three individual models with four different sizes of delamination radius (i.e. $\alpha = 0$, 0.1, 0.3 and 0.6). The delamination surfaces are modelled by lines of overlapping nodes with frictionless contact between delaminated surfaces. A biased mesh was used near the delamination boundaries in order to acquire more accurate results. Load was calculated from the uniform pressure, and displacement was taken as the deflection of the bottom most node at the bottom sublaminate. A single degree of freedom linear spring element with zero initial length and stiffness of 10^5 *N/mm* was used to connect nodes at the 'crack tip' to quantify the Mode II strain energy using the relative nodal displacements and spring force. The numerical strain energy release rate from these models is compared with the theoretical solution in the following sections.

5 Analytical Results and Discussions

5.1 Full Non-dimensional Solutions

Results based on the governing Eq.17 are presented in this section to identify the key parameters for the severity of multiple delaminations in a fixed circular plate under transverse loading. Using the γ value from the thin circular plate theory (i.e. $\gamma = 3$), the coefficient of the linear term in Eq.3 is obtained for the circular plate with a fixed boundary. Non-dimensional loads are plotted in Figure 6 against normalized displacements for an undamaged circular plate. The numerical stiffness of the plate is obtained from the finite element analysis. The analytical solution from Eq.2 is in agreement with the finite element results when $k = 0.4$. The coefficients $\gamma = 3$ and $k = 0.4$ are therefore chosen for the load-displacement relation in both the global plate (Eq.2) and delaminated portion (Eq.4).

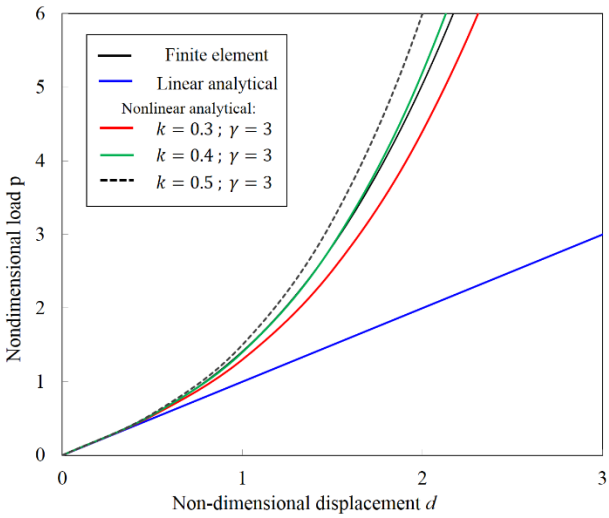

Figure 6: Linear and nonlinear relation between the normalised load and deflection for the fixed circular plate with different k coefficient obtained by Eq.2 and the axisymmetric finite element model.

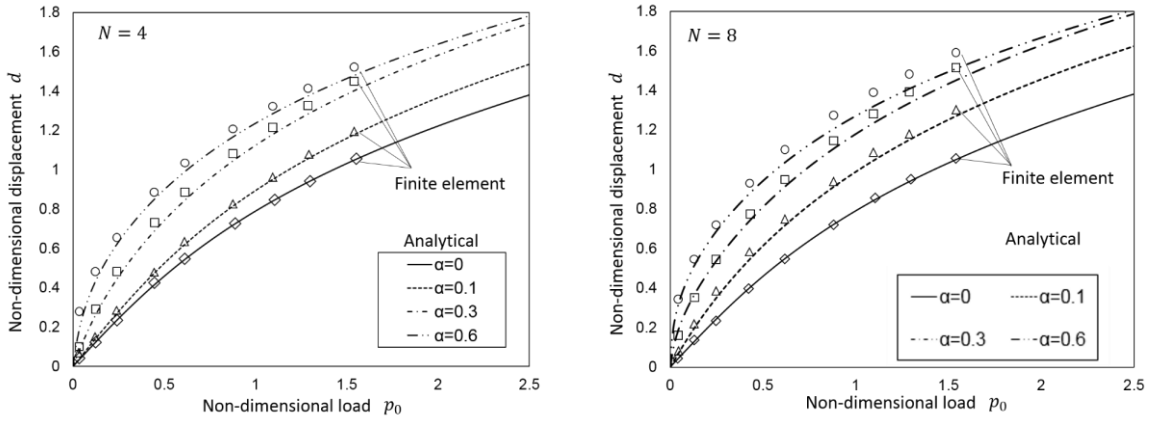

(a) (b)

Figure 7: Comparison of non-dimensional load and displacement relation for circular plate with (a) N = 4 and (b) N = 8 and finite element modelling results with increasing delamination radius a.

The normalised (non-dimensionalised) relations between applied load (p_0) and displacement (d where $d=\delta/h$) for the fixed circular plates with four delamination sizes α = 0, 0.1, 0.3 and 0.6 obtained by the present theory (based on Eq. 17) are compared with the finite element results in Figure 7. These figures show the significance of the geometric nonlinearity associated with multiple delaminations in the load-displacement relations with increasing delamination size. The level of nonlinearity increases with the size of delaminations and the number of delaminations for a given normalised load level. There is good agreement with the finite element solutions. The nonlinearities of the finite element model are slightly higher compared to the analytical solutions when the delamination size and number are large. This

could possibly be because the approaches used for deflection measurement are different. However, the general trend of plates with different delamination sizes is well captured by the analytical models. When comparing the load-displacement relations of laminates with different numbers of delaminations (i.e. $N = 4$ and $N = 8$) for a given delamination size, no significant differences can be found except for the case when $\alpha = 0.1$, which shows that once delamination is present, the influence of the number of delaminations, for a given delamination size, is less important. The nonlinearity of laminate with $N = 8$ appears to be higher than that of laminate with $N = 4$. The comparison of the numerical analysis shows that the present solution is valid to represent the load-displacement relation in cases of multiple delaminations, i.e. the damage accumulation behaviour due to indentation and large mass low velocity impact.

Figure 8 shows the variation of s with overall displacement level and increasing delamination size for the $N = 4$ and $N = 8$ cases. It is noted that the s and d are normalised by t and h, respectively. It can be seen that s appears to be almost constant and insensitive to the overall deflection when the delamination is small (i.e. when $\alpha \leq 0.1$). As the delamination grows from $\alpha = 0.1$ to 0.3, the increase in s is dramatic. In addition, for a given overall deflection level, the laminates with $N = 8$ have a relatively larger s value compared to laminates with $N = 4$. Therefore, the number of delaminations also significantly influences the initial local deflection of the global plate.

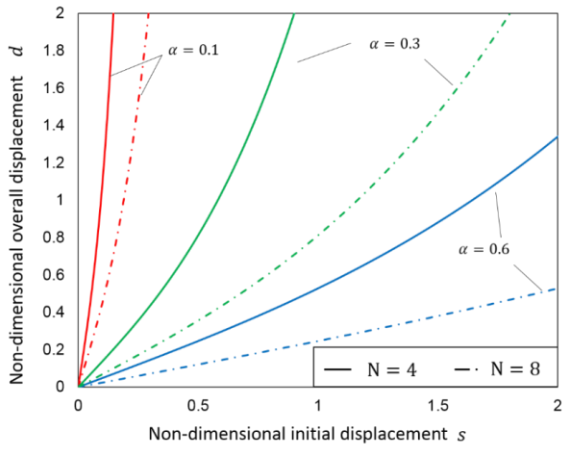

Figure 8 Relation between initial defection of global plate (s) and overall defection (d) in plates with $N = 4$ and $N = 8$.

In the low-velocity impact and static indentation tests, after the initial delamination is induced, delamination growth is a fairly stable process, which can be considered as an equilibrium condition and solved by the closed-form formulae.

Figure 9 compares the two equilibrium paths associated with delamination propagation when G_{IIC} = 0.8 *N/mm* in laminates with N = 4 and 8, and the same delamination sizes are marked on each curve. 0.8 *N/mm* was also used in [6]. The two cases of N = 4 and 8 are representative of the Ps and Ss laminates if considering each N as a sublaminate group of [45°/0°/90°/-45°] plies. The overall load-displacement curves of the laminates with N = 4 and N = 8 are quite similar after delamination initiation, which implies that the normalised strain energy available for delamination propagation of both cases is similar. Because of the difference in the number of delaminations between the two cases, the delamination size growth rate in the laminate with N = 8 is slower than in the laminate with N = 4. This suggests that the strain energy available is relatively insensitive to the number of delaminations in the given condition. This is backed up by the experimental observations of the close similarities in level of nonlinearity between the Ps and Ss cases in scaled indentation experiments [6].

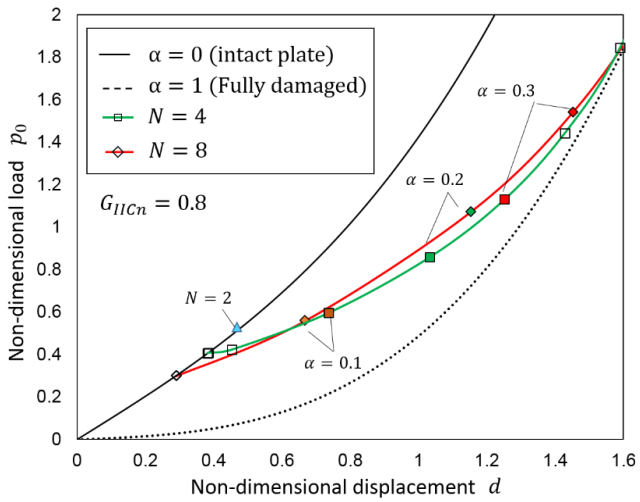

Figure 9 Comparison of normalised load-displacement curves of plates with N = 4 and N = 8 and with constant non-dimensional critical strain energy release rate

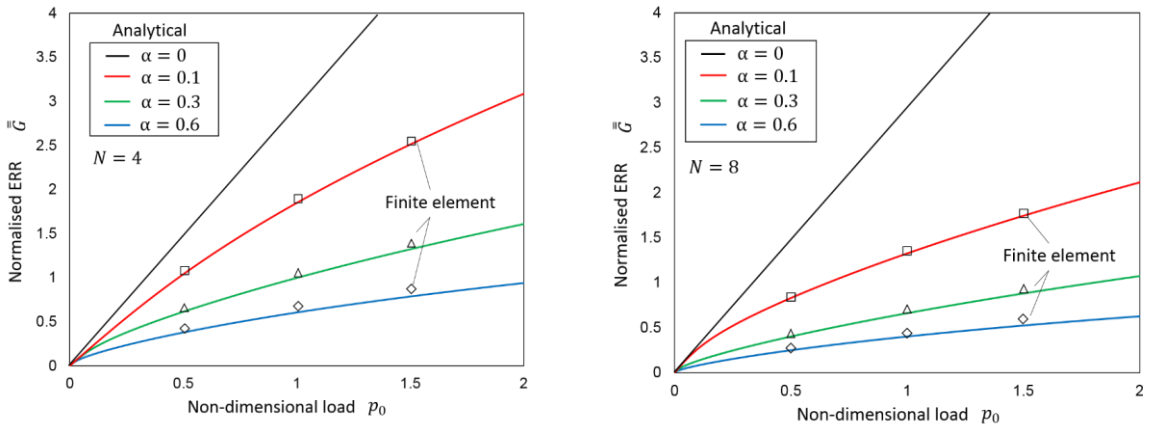

(a) (b)

Figure 10 Variation of normalised strain energy release rate with normalised load for plate with (a) N=4 and (b) N=8 as increasing delamination area. Results from finite element models are compared against theoretical value for each case.

The normalised strain energy release rate (ERR), $\bar{\bar{G}} = \sqrt{\bar{G}}$, normalised by the critical value is plotted against the applied normalised load for cases of α = 0, 0.1, 0.3 and 0.6 when N = 4 and 8 in Figure 10a and b, respectively. These figures show that the larger the delamination radius α is, the less the strain energy release rate increases with load. This tendency is more obvious when the delamination number N is large. This is because the membrane component becomes dominant with increasing delamination size and number, and the effect of the delaminations' growth on the stored strain energy release rate decreases. The load must therefore be increased to keep the delaminations growing. The current solution again is in good agreement with the finite element results.

5.2 Analytical Modelling of Scaled Indentation Test

The predicted load-displacement relations were derived analytically for the experimental study in reference [6], using the full analytical expressions (based on Eq.17) including geometric nonlinear effects in both the global intact plate and delaminated portion as well as the initial local deflection (s) for each laminate configuration (see Table 1). In order to fully apply the theoretical solutions developed so far, it is additionally necessary to account for the boundary conditions and determine an equivalent radius for the rectangular shaped plates. The solution applied also allowed for simply supported boundary conditions for the global plate, whilst the fully constrained condition for local delaminated portion remains the same. The method is modified from the clamped circular plate, with the size of the plate corrected in order to fit the deflection field of the simply supported rectangular plate by comparing two analytical solutions. The radius of the equivalent circular large plates (the Is, Ps and Ss cases) and the reference plate was corrected to 70 mm and 35 mm, respectively. Dimensions used for the four scaled laminates in the analytical modelling can be found in Table 2. To account for the effects of orthotropic laminates on indentation response, the bending stiffness of isotropic material D used throughout in the analytical approach was replaced by the effective bending stiffness D^* obtained from [27] considering orthotropy of the laminate.

Comparison between experimental result and analytical solution for each laminate configuration is shown in Figure 11; the damage initiation point (when $\alpha \rightarrow 0$) for each case is marked in red. It was assumed that the N value represents the number of stacking groups of

[45°/0°/90°/-45°], which is frequently used to approximate the number of circular delaminations in laminated composite under transverse loading in the literature [8,21]. In order to be consistent between the Ps and Ss cases, $N = 8$ was used for the Ss case and $N = 4$ was applied for the rest of the laminates. Table 3 shows the total, projected and experimentally derived averaged N values from the experimental results (CT-scan) across the four scaled laminates from [6]. It can be seen that the experimental N value for all cases are roughly similar and close to '4'. $N = 8$ is used for the Ss case as it has twice number of stacking groups as the rest of the cases.

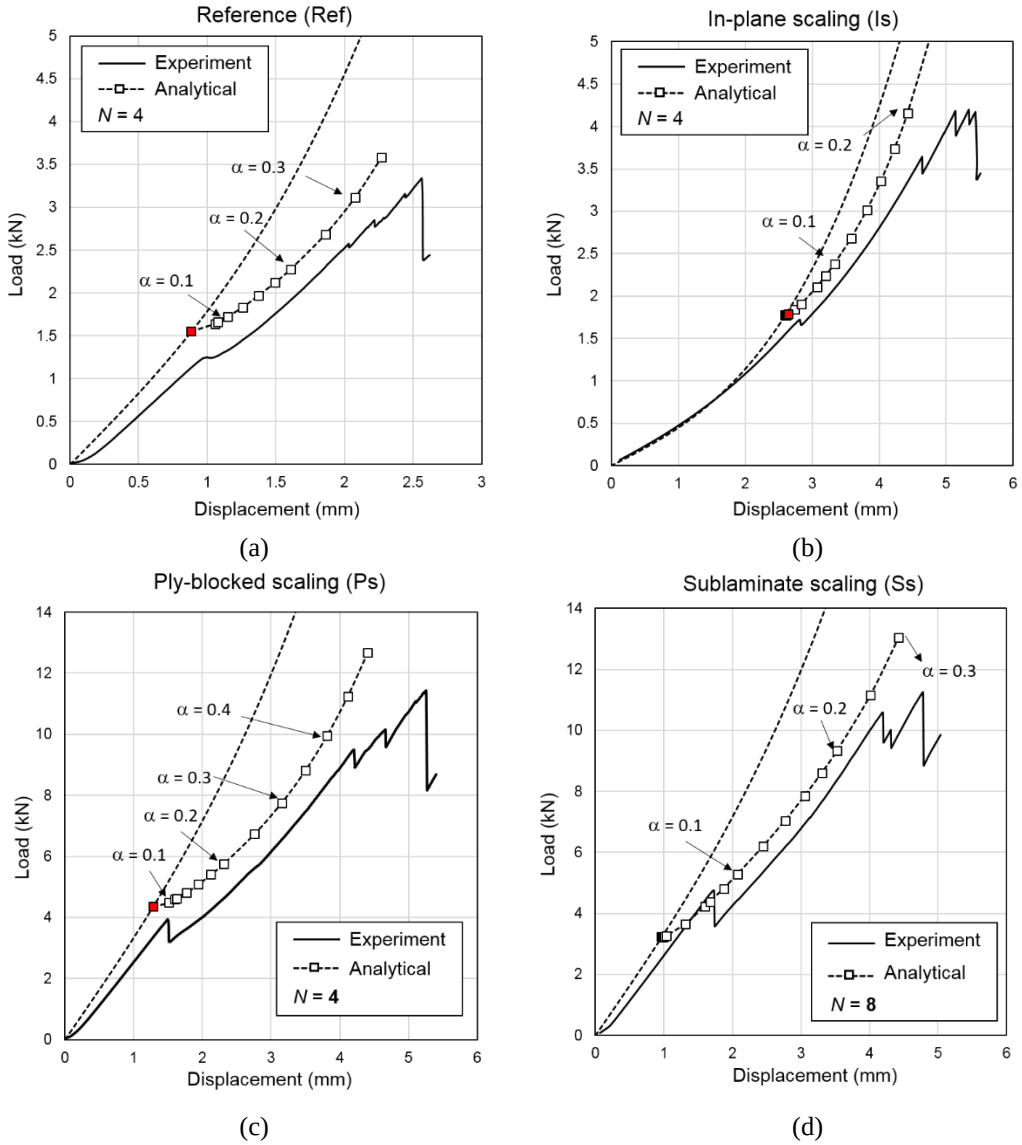

Figure 11: Comparison of experimental results and full analytical solution (based on Eq. 17) for each laminate configuration tested, with indication of delamination ($\alpha = a/R$) growth as load increases. (a) Reference laminate; (b) In-plane scaling laminate; (c) Ply-blocked scaling laminate;

(d) Sublaminate scaling laminate. Damage initiation data point for each analytical solution is marked in red.

Table 2 Dimensions used for modelling scaled laminates under transverse point loading using full analytical expressions. ($t_{theo} = N/h$).

Laminate configurations	D^* (kN·m)	N	h (mm)	$t_{theo.}$ (mm)	Actual In-plane simply supported size (mm)	Equivalent clamped circular plate radius (mm)
Reference (Ref)	45.6	4	2	0.5	37.5 x 62.5	35
In-plane scaling (Is)					75 x 125	70
Ply-blocked scaling (Ps)	364.5		4	1		
Sublaminate-scaling (Ss)		8		0.5		

As shown in Figure 11, analytical solutions also show good agreement with experiment results for both the general trend and nonlinearity during delamination propagation for most of the cases. Similar to what is presented in [6], and using nonlinear force-displacement expressions based on circular plate theory, the overestimations of initial stiffness presented here are also caused by the assumption of equivalent circular plate, as well as the indentation effect in the experiment. Despite these overestimates, the analytically derived stiffnesses during delamination propagation (i.e. $\alpha > 0$) for each case are in good agreement with the experimental results. It can be found that the delamination growth of the Ss case is much slower due to a higher N value compared to the Ps case for given indentation load, which is again in line with the experimental observations presented in [6]. In general, the load-displacement relation across the four scaled laminates are well captured by the analytical solution. For more accurate analysis, the full stiffness matrix and the actual dimensions of the laminates should be taken into account [28].

Table 3: Experimental results of delamination areas and N value of the four scaled laminated in [6]. Note that the experiment N value is calculated by total delamination area divided by projected delamination area for each case.

Laminate configurations	Exp. total delamination area (mm^2)	Exp. projected delamination area (mm^2)	Exp. N value
Reference (Ref)	106	34	3
In-plane scaling (Is)	147	57	3
Ply-blocked scaling (Ps)	666	142	5
Sublaminate-scaling (Ss)	1188	300	4

The sudden load drops at damage initiation were not able to be modeled with the current analytical solution in a single step as there are two equilibrium states. Prediction of the level of the initial load drop for laminated composites under transverse loading due to delamination onset, which is an unstable event, is an important topic for scaling tests and has not been quantitatively addressed in the literature.

Plate behaviours before and after the critical load of indentation/impact can be considered as two equilibrium stages. If assuming a constant critical strain energy release rate for delamination initiation and propagation, it can be considered that the load drop at damage onset is the result of unstable delamination propagation, i.e. a 'jump' between two equilibrium paths at constant displacement. This constant displacement is considered as a critical displacement. Therefore, one can approximate the load drop and complete indentation/impact loading process by the superposition of two equilibrium paths (before and after delamination propagation), which is here called the '*superposition method*'. The level of load drop can be derived as the difference between the critical load on the first equilibrium path and the load corresponding to the critical displacement on second equilibrium path. The displacement level is that at which P_C in Eq. 19 is reached, when $N = 2$. This interpretation is backed up by the high-fidelity modelling results presented in [29]. The maximum interlaminar stresses are at the mid-plane of the laminate before the critical load during indentation and the high-fidelity FE models showed the first delaminations to occur at interfaces near the mid-plane, which is similar to the scenario when $N = 2$. Then, the FE prediction showed delaminations migrating and propagating into multiple interfaces (i.e. when $N > 2$, giving $N = 4$ or 8 as previously assumed). Therefore, the initial behaviour of the plate can be represented by an intact global plate under concentrated load as per the above analysis (see Figure 11); the load drop is modelled by joining the two equilibrium paths, $N = 2$ with $\alpha \rightarrow 0$ and $N = 4$ for the Ref, Is and Ps cases and $N = 8$ for the Ss case, at the critical displacement.

Figure 12 compares the experimental results and analytical results using the newly proposed superposition method. In general, the analytical solution using the superposition method gives good approximations for the cases compared. In addition, predictions of the level of load drop (ΔP) and delamination size (α) corresponding to the critical load (initial delamination size) are available. It seems that the response of the Ref plate is sufficiently well modelled using only the equilibrium path of $N = 4$ (see Figure 11a) as no significant load drop was observed in this experimental case. The difference between the levels of load drop of the Ps and Ss cases suggests the level of load drop depends on the number of interfaces available

for delaminations (i.e. *N* value). The same observation has been found in similar tests in the literature [30,31]. Multiple delaminations accompanied by extensive matrix cracks were observed for all types of laminates. Given that both analytical solutions, based on a single equilibrium path and the superposition method, correlate with experimental results well (see Figure 11 and Figure 12), it can be confirmed that although matrix cracks help delamination migration , their effects on the global behaviour are insignificant.

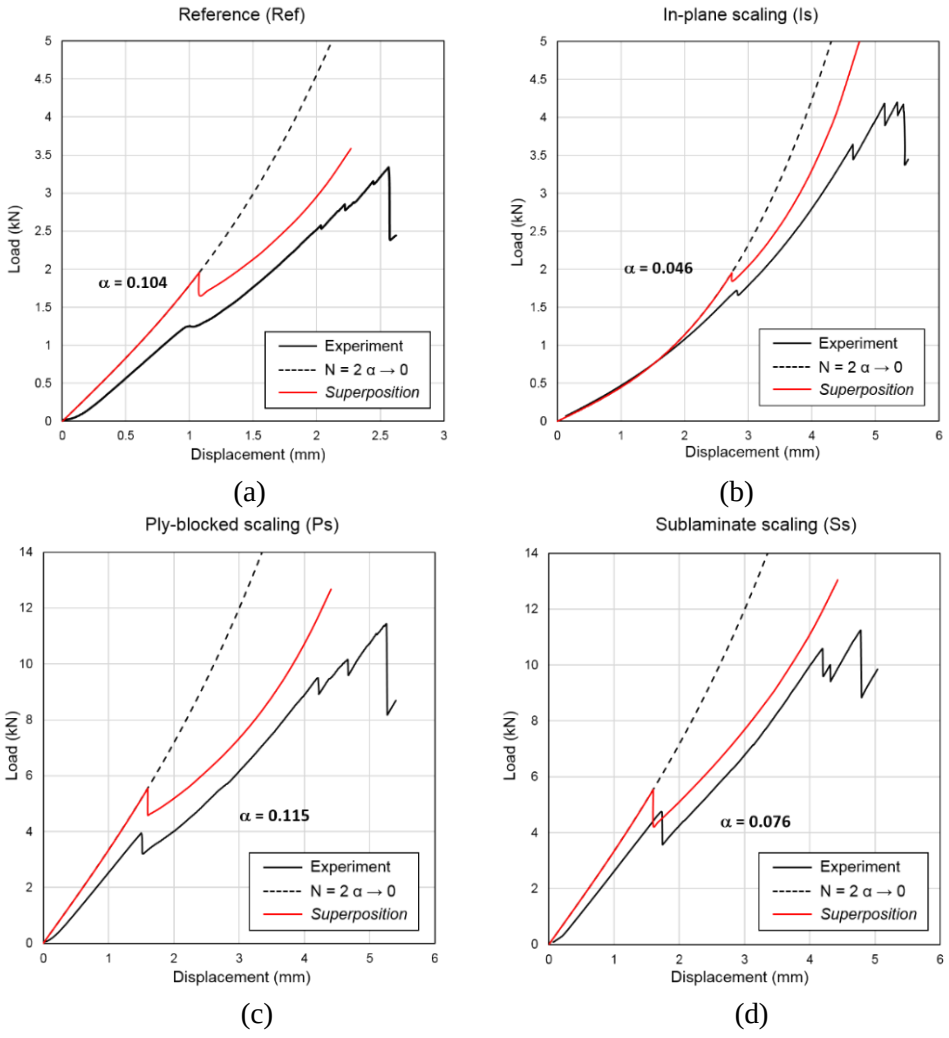

Figure 12: Comparison of experimental results and analytical results using superimposing of two equilibrium paths. (a) Reference case, (b) Ply-blocked case and (c) Sublaminate scaling case.

Table 4: Experimental and analytical results of load drop level and initial delamination size.

Laminate configurations	*N* value used for superposition method	Exp. load drop (N)	Theo. load drop (N)	Exp. initial delamination Dia. (mm)	Theo. initial delamination Dia. (mm)
Reference	4	44.8	299.1	6.6	7.8

In-plane scaling		62.9	112.4	8.5	6.9
Ply-blocked scaling		831.6	956.2	13.5	17.3
Sublaminate-scaling	8	1164.4	1316.1	19.5	11.4

Table 4 lists the experimental and analytical results from the superposition method. The predictions of the level of load drop are in good agreement with the experimental results for the Ps and Ss cases. Again, the Ref case can be better modelled using only the $N = 4$ equilibrium path without modelling the load drop. When comparing the Ps and Ss cases, the initial delamination area predicted for the Ss plate is 30% smaller than the Ps case. This is because of the higher N value and critical load for the Ss case compared to the Ps case and the delayed delamination growth in the Ss case (see

Figure 9, and Figure 11 c and d). The analytical results for the initial delamination size scaling (ratio of initial delamination size) of the truly scaled pair of laminates (i.e. the Ref and Ps cases), roughly agrees with the experiment result; and it gives a scaling factor of 2.2.

The superposition method is the solution that is best for capturing the overall behaviour of the plates, but the damage predictions are highly dependent on the choice of N. Moreover, the boundary condition assumed for the delaminated portion being fully clamped could fall short when the delamination size is small. Thus, it may not be sufficient to quantitatively compare the estimates with the experimental results of delamination size across all laminate types. In general, the superposition method describes the overall load-displacement curve very well for the Ps and Ss cases, and it provides reasonable approximations on the level of critical load and order of magnitude of initial delamination size for most of the cases.

The geometric nonlinearity associated with multiple delamination propagation may unnecessarily over complicate most of the cases, except for the Is plate. The other cases do not exhibit strong geometric nonlinearity before and right after the load drop (see Figure 11 and Figure 12). It therefore allows one to apply a simplified expression to the truly scaled pair (the Ref and Ps case) to obtain the level of load drop. The level of load drop can be simply treated as the difference between critical loads when $N = 2$ and $N = 4$ based on Eq.19. This yields:

$$\Delta P = \sqrt{\frac{32\pi^2 D^* G_{IIC}}{3}} - \sqrt{\frac{32\pi^2 D^* G_{IIC}}{6}} = \sqrt{\frac{32\pi^2 D^* G_{IIC}}{3}}\left(1 - \frac{1}{\sqrt{2}}\right) \approx 0.26 P_C \qquad (25)$$

Compared to the experimental values, Eq.25 appears to give a reasonable estimate of the load drop for the thick Ps plate, while it greatly overestimates the experimental response for the thin Ref plate, which is similar to the results of the improved solution.

The above approaches provide useful insights into the nonlinear load-displacement response of scaled laminates and scaling mechanisms involved. However, there seems no single analytical method available to predict all the experimental results in full. This may be attributed to the limitations of the assumptions made in using thin plate theory of isotropic plates. To improve this modelling, the high-fidelity numerical models that are presented and validated in [29] are required, where the damage is explicitly modelled by formulations based on combined stress and fracture energy criteria, and the effects of nonlinearity, boundary conditions and delamination on the response of laminate under transverse loading are fully captured.

6 Conclusions

An analytical approximation based on plate theory and its application were presented in this study, it was validated against numerical simulation and applied to investigate scaled laminates under transverse loading. Different simplification approaches were presented and shown to be suitable for various scenarios. In general, results show the significance of the geometric nonlinearity associated with multiple delaminations in the load-displacement relations with increasing delamination size for laminates under transverse loading. The level of nonlinearity increases with the size of delaminations and the number of delaminations. The load drop in a laminate's response to transverse loading and associated initial delamination was modelled with a combination of two equilibrium analytical solutions, and comparison was made with numerical and experimental results. It was found that the solution is highly dependent on the value chosen for N, as this value governs the starting point of unstable delamination propagation. The analytical results correlate very well with the experimental results when $N = 2$, whilst the estimations when $N > 2$ appear to fall below for the experimental critical load. The superposition method is able to accurately capture the full nonlinear response across all laminate configurations tested, as well as the level of load drop. Although it is difficult to derive a single closed-form analytical method to interpret all experimental observations for all laminate configurations, analytical approaches based on plate theory were generalised and discussed here. These analytical solutions complement the advanced finite

563 element analysis solutions presented in [5,29] which investigate the full damage behavior and
564 structural scaling effects.

565 **7 References**

566 [1] Sun XC, Hallett SR. Failure mechanisms and damage evolution of laminated composites
567 under compression after impact (CAI): Experimental and numerical study. Compos Part
568 A Appl Sci Manuf 2018;104:41–59.
569 [2] Shi Y, Swait T, Soutis C. Modelling damage evolution in composite laminates subjected
570 to low velocity impact. Compos Struct 2012;94:2902–13.
571 [3] Lopes CS, Camanho PP, Gürdal Z, Maimí P, González EV. Low-velocity impact
572 damage on dispersed stacking sequence laminates. Part II: Numerical simulations.
573 Compos Sci Technol 2009;69:937–47.
574 [4] Maimí P, Camanho PP, Mayugo J a., Dávila CG. A continuum damage model for
575 composite laminates: Part II – Computational implementation and validation. Mech
576 Mater 2007;39:909–19.
577 [5] Sun XC, Hallett SR. Barely Visible Impact Damage in Scaled Composite Laminates:
578 Experiments and Numerical Simulations. Int J Impact Eng 2017;109.
579 [6] Abisset E, Daghia F, Sun XC, Wisnom MR, Hallett SR. Interaction of inter- and
580 intralaminar damage in scaled quasi-static indentation tests: Part 1 – Experiments.
581 Compos Struct 2016;136:712–26.
582 [7] Serra J, Bouvet C, Castanié B, Petiot C. Experimental and numerical analysis of Carbon
583 Fiber Reinforced Polymer notched coupons under tensile loading. Compos Struct
584 2017;181:145–57.
585 [8] Suemasu H, Majima O. Multiple Delaminations and their Severity in Circular
586 Axisymmetric Plates Subjected to Transverse Loading. J Compos Mater 1996;30:441–
587 53.
588 [9] Abrate S. Impact on composite structures. Cambridge University Press; 2005.
589 [10] Olsson R. Impact Response of Composite Laminates: A Guide to Closed Form Solutions.
590 Aeronautical Research Institute of Sweden; 1993.
591 [11] Christoforou AP, Yigit AS. Characterization of impact in composite plates. Compos
592 Struct 1998;43:15–24.
593 [12] Lin C, Fatt MSH. Perforation of Composite Plates and Sandwich Panels under Quasi-
594 static and Projectile Loading. J Compos Mater 2006;40:1801–40.
595 [13] Abrate S. Modeling of impacts on composite structures. Compos Struct 2001;51:129–
596 38.
597 [14] Wu E, Yen C-S. The Contact Behavior Between Laminated Composite Plates and Rigid
598 Spheres. J Appl Mech 1994;61:60.
599 [15] Olsson R, Nilsson S. Simplified prediction of stresses in transversely isotropic
600 composite plates under Hertzian contact load. Compos Struct 2006;73:70–7.
601 [16] Suemasu H, Kerth S, Maier M. Indentation of Spherical Head Indentors on Transversely
602 Isotropic Composite Plates. J Compos Mater 1994;28:1723–39.
603 [17] Esrail F, Kassapoglou C. An efficient approach to determine compression after impact
604 strength of quasi-isotropic composite laminates. Compos Sci Technol 2014;98:28–35.
605 [18] Kassapoglou C. Modeling the Effect of Damage in Composite Structures: Simplified
606 Approaches. John Wiley & Sons; 2015.
607 [19] Davies GAO, Robinson P, Robson J, Eady D. Shear driven delamination propagation in
608 two dimensions. Compos Part A Appl Sci Manuf 1997;28:757–65.

[20] Schoeppner GA, Abrate S. Delamination threshold loads for low velocity impact on composite laminates. Compos Part A Appl Sci Manuf 2000;31:903–15.
[21] Suemasu H, Majima O. Multiple Delaminations and their Severity in Nonlinear Circular Plates Subjected to Concentrated Loading. J Compos Mater 1998;32:123–40.
[22] Olsson R, Donadon M V., Falzon BG. Delamination threshold load for dynamic impact on plates. Int J Solids Struct 2006;43:3124–41.
[23] Suemasu H, Wisnom MR, Sun XC, Hallett SR. An analytical study on multiple delaminations and instability in nonlinear plate subjected to transverse concentrated load. 13th Japan Int SAMPE Symp Exibition 2013.
[24] Suemasu H, Wisnom MR, Sun XC, Hallett SR. Damage Estimation in Nonlinear Laminates Subjected to a Transverse Concentrated Load. 20th Int. Conf. Compos. Mater., 2015, p. 19–24.
[25] Olsson R. Impact response of orthotropic composite plates predicted from a one-parameter differential equation. AIAA J 1992;30:1587–96.
[26] Eduard Ventsel TK. Thin Plates and Shells: Theory: Analysis, and Applications. CRC Press; 2001.
[27] Olsson R. Low- and medium-velocity impact as a cause of failure in polymer matrix composites. Fail Mech Polym Matrix Compos Criteria, Test Ind Appl 2012:53–78.
[28] Matsuhashi H, Graves M, Dugundji J, Lagace P. Effect of membrane stiffening in transient impact analysis of composite laminate plates. 34th Struct. Struct. Dyn. Mater. Conf., Reston, Virigina: American Institute of Aeronautics and Astronautics; 1993.
[29] Sun XC, Wisnom MR, Hallett SR. Interaction of inter- and intralaminar damage in scaled quasi-static indentation tests: Part 2 – Numerical simulation. Submitt to Compos Struct 2015;136:727–42.
[30] Nettles A, Douglas M. A comparison of quasi-static indentation to low-velocity impact. NASA Tech Rep 2000;NASA/TP-20.
[31] Yokozeki T, Kuroda A, Yoshimura A, Ogasawara T, Aoki T. Damage characterization in thin-ply composite laminates under out-of-plane transverse loadings. Compos Struct 2010;93:49–57.